Sensors and Actuators B 196 (2014) 23–30

Contents lists available at ScienceDirect

Sensors and Actuators B: Chemical

journal homepage: www.elsevier.com/locate/snb

Investigation and cancellation of residual amplitude modulation in fiber electro-optic modulator based frequency modulation gas sensing technique

Zhixin Li, Longhui Zhao, Wei Tan, Weiguang Ma*, Gang Zhao, Xiaofang Fu, Lei Dong, Lei Zhang, Wangbao Yin, Suotang Jia

State Key Laboratory of Quantum Optics and Quantum Optics Devices, Institute of Laser Spectroscopy, Shanxi University, Taiyuan 030006, China

ARTICLE INFO

Article history:
Received 15 November 2013
Received in revised form 3 January 2014
Accepted 30 January 2014
Available online 6 February 2014

Keywords:
Frequency modulation spectroscopy
Trace gas detection
Residual amplitude modulation
Polarization detection
Servo control

ABSTRACT

Frequency modulation spectroscopy (FMS) is most commonly used for trace gas detection, but its sensitivity is usually limited by the background noise attributed to residual amplitude modulation (RAM). In this paper, comprehensive theoretical analyses of FMS with and without RAM are presented. Then the measurements of RAM are experimentally verified utilizing a fiber electro-optic modulator based FMS setup. In order to reduce the RAM, a novel servo control method with its correction signal obtained from a polarization detection scheme was proposed and pure FMS signals of C_2H_2 gas at wavenumber of 6544.4419 cm^{-1} are obtained. Furtherly, long-term measurements of the dispersion background signal with feedback loop on and off are performed to evaluate the stability of the instrument. Finally, this servo control method is extended into the application of Pound–Drever–Hall frequency stabilization technique to improve the locking accuracy and stability.

Introduction

The highly sensitive frequency modulation spectroscopy (FMS) is proposed by Bjorklund [1] for the detection of weak transitions and independently by Drever and Hall [2] for laser frequency stabilization based on the detection of the reflected field of a Fabry–Perot cavity. FMS has potentials to reach the shot noise limit [3,4] and has been applied to many fields such as trace gas detection [5,6], optical frequency standards [7,8], and laser interferometers [9]. However, the theoretical shot-noise-limited sensitivity of FMS is usually not achieved since the limitation of residual amplitude modulation (RAM) induced in the frequency modulation (FM) process [10].

Basically, the RAM appears at modulation frequency when the modulated sidebands are not exactly equal in magnitude and opposite in phase. The balance of sidebands can be easily destroyed by the polarization variation of laser output, temperature-dependent birefringence of the electro-optic (EO) crystal, polarization mode dispersion (PMD) of the transmission fiber, etalon effect due to the crystal's or other reflective surfaces, amplitude fluctuation of the radio frequency (RF) power, and frequency fluctuation of the laser. However, all these factors vary as a function of time. As a result, the detection of this amplitude modulation leads to a non-zero dispersion baseline fluctuated in time and a distortion of FMS signal, which limits the detection sensitivity of FMS strongly [11]. When a waveguide-type of fiber coupled electro-optic modulator (*f*-EOM) is used to modulate the laser light, the effect of multiple reflections is negligible. The focus of this work is to demonstrate and eliminate the RAM induced by the phase mismatch of the propagated light in a birefringent material.

In the application of FMS to trace gas detection, several techniques have been developed to eliminate the influences of RAM caused by the phase mismatch. One approach was careful and periodic adjustment of the relevant optical parameters [12,13]. This passive control method is inconvenient and inadequate when the signal is weak. Levenson et al. reported a quantum-noise-limited performance of FMS using a second modulation to modulate the optical heterodyne signal at a frequency higher than that of RAM noise spectrum [14]. Wong and Hall obtained a correction signal through demodulating the detected signal without absorption after the EOM and then feedback it to EOM to suppress the generation of RAM [15]. In 1986, a two-tone optical heterodyne spectroscopy was developed by Cooper et al. with a diode laser [16]. In this technique, the beam was modulated at two distinct frequencies and the signal was detected at the difference frequency which was insensitive to RAM. Kasapi et al. performed FMS with a sub shot-noise background in rubidium detection based on diode laser, in which the RAM rejection was achieved by an injection locking technique [17].

* Corresponding author. Tel.: +86 3517018904; fax: +86 3517018927.
E-mail address: mwg@sxu.edu.cn (W. Ma).

0925-4005/$ – see front matter © 2014 Elsevier B.V. All rights reserved.
http://dx.doi.org/10.1016/j.snb.2014.01.111

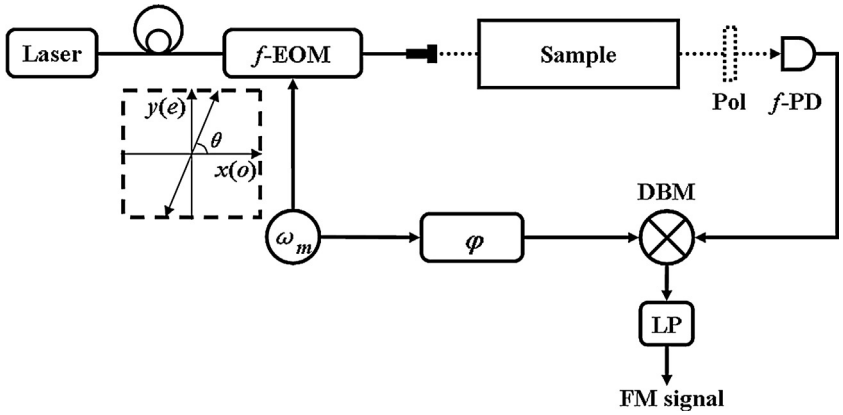

Fig. 1. Schematic diagram of the FMS technique based on a fiber EOM. *f*-EOM—fiber electro-optic modulator; Pol—polarizer; *f*-PD—fast response photodetector; LP—low-pass filter; DBM—double balanced mixer; ω_m—radio frequency.

Foltynowicz et al. reduced the RAM background signal significantly in noise-immune cavity-enhanced optical heterodyne molecular spectroscopy (NICE-OHMS) through two different strategies, one of which was using an *f*-EOM with a titanium diffused waveguide and an active feedback control technique similar to the Wong–Hall method, the other was using an *f*-EOM with a proton exchanged waveguide that does not support light propagation along the ordinary (*o*-)axis [18]. Recently, a new servo control method based on a polarization detection scheme and a *f*-EOM was developed by our group to ensure a high degree of linear polarization output from a polarization-maintaining (PM) fiber, and the work also showed us a prospect that the scheme could be used for the application of RAM reduction in FMS [19].

In this paper, the production principle and evaluation of RAM in *f*-EOM based FMS is described in detail firstly, and then a novel servo control method based on a polarization detection scheme is proposed to reduce RAM. The correction signal is obtained through detecting the polarization state variation of laser beam output from the modulator and then feedback this signal to the *f*-EOM to suppress the generation of RAM. Comparing to the above mentioned methods, the new proposed scheme can be implemented without extra modulation and demodulation. In addition, the proposed scheme is used in the PDH frequency stabilization technique for optimization.

Theoretical analysis

Pure FM spectroscopy

The schematic diagram of FMS technique is shown in Fig. 1. The light emission of the laser is led through an EOM, in which the light field is modulated at a radio frequency (RF) ω_m. In this scheme, an *f*-EOM, with the electronic modulation signal applied along the extraordinary (*e*-)axis of the EO crystal, is employed rather than a free-space EOM because of the attractive advantages in its wide working frequency range, low half wave voltage, and small size.

The output of the modulated light beam can be described by a strong carrier at frequency ω_c and two weak sidebands at frequencies $\omega_c \pm \omega_m$, where one in phase and one out of phase with the carrier. Then the beam emerging from the modulator passes through an absorption cell and impinges on a fast-response photodetector (*f*-PD). The detected signal is demodulated with a reference signal by a double balanced mixer (DBM). With the high frequency components filtered out by a low-pass filter, the FM signal can be obtained as [20]

$$I_{\mathrm{FM}} = I_0 J_0(\beta) J_1(\beta) e^{-2\delta_0} \left[(\delta_{-1} - \delta_1) \sin\theta_{fm} + (\phi_1 + \phi_{-1} - 2\phi_0) \cos\theta_{fm} \right], \quad (1)$$

where I_0 is the initial intensity of unmodulated beam, $J_n(\beta)$ is the Bessel function of order n, and β is the FM index. $\delta_{0,\pm1}$ and $\phi_{0,\pm1}$ represent the amplitude attenuation and phase shift at center frequencies of ω_c, $\omega_c \pm \omega_m$, respectively. θ_{fm} is the detection phase defined as the phase difference between the detected signal and the reference signal. In Eq. (1), the square bracket is composed of the $\sin\theta_{fm}$ and $\cos\theta_{fm}$ terms, the front parts of which are referred as the absorption and dispersion signals, respectively. By adjusting the detection phase, the FM signal can thus be pure absorption, pure dispersion, and a combination of them.

General FMS with RAM contained

The above discussed pure FM signal is obtained under ideal conditions, and it is clear that the detected FM signal should be zero when there is no sample absorption. However, when the polarization of the light impinging upon the EOM is not linear or not aligned properly, the balance of the FM triplet output from the EOM will be destroyed and results in the generation of RAM. Especially for an *f*-EOM, the imperfect alignment between the fiber connectors and the birefringence effect of fiber core could make the RAM even seriously. It is worth noting that there could be a residual modulation along the *o*-axis if the electric field is not strictly parallelized to the *e*-axis of EO waveguide [21], but this modulation can be neglect in our case since the modulation amplitude is more than 5 times smaller than that along the *e*-axis [22]. As a result, the general FMS with RAM contained based on an *f*-EOM is theoretically analyzed just considering the modulation along the *e*-axis as flows.

The illustration in the inset of Fig. 1 shows the coordinate sets and the orientations of the principle axes of the fiber and crystal. Since the misalignment of the principle axes of the fibers and EO crystal has been reduced as small as possible (smaller than 3°) in the factory mounting [22], we assume that the *e*- and *o*-axes of the input PM fiber and those of the *f*-EOM possess the same directions and they are parallel to *x*-axis and *y*-axis, respectively. The laser propagates along the *z*-axis which is perpendicular to the *x*–*y* plane. Consider a linear polarized laser radiation incident with frequency ω_c and amplitude E_0.When the polarization direction of incident light has an angle of θ with respect to the *x*-axis (i.e., *o*-axis of the

PM fiber and *f*-EOM), the light field in the form of Jones vector can be written as

$$\hat{E} = \begin{pmatrix} \cos\theta \\ \sin\theta \end{pmatrix} E_0 e^{-i\omega_c t} \tag{2}$$

The Jones matrix of the *f*-EOM can be given by

$$J_{EOM} = \begin{pmatrix} 1 & 0 \\ 0 & e^{i(\Delta\varphi+\Delta\phi+\phi_{dc}+\beta\sin\omega_m t)} \end{pmatrix}, \tag{3}$$

where $\Delta\varphi = \varphi_o - \varphi_e$ and $\Delta\phi = \phi_o - \phi_e$ are the phase differences between the slow and fast axes of the PM fiber and the EOM crystal, respectively, which can be changed by temperature. ϕ_{dc} is the phase shift induced by the DC voltage applied to *e*-axis of the EO crystal. After the *f*-EOM, the electric field can be written as

$$\begin{pmatrix} E_x \\ E_y \end{pmatrix} = J_{EOM}\hat{E} = \begin{pmatrix} \cos\theta \\ \sin\theta e^{i(\Delta\varphi+\Delta\phi+\phi_{dc}+\beta\sin\omega_m t)} \end{pmatrix} E_0 e^{-i\omega_c t} \tag{4}$$

Since normal optical mirror or glass shows polarization selection properties to some extent, the analysis is given based on an additional assumed polarizer. If this assumed polarizer provides an angle of γ with respect to *e*-axis of *f*-EOM and the Jacobi Anger expansion is used, the electric impinged on the detector can be calculated as

$$\begin{aligned} E_{FM} &= \left(\cos\theta\sin\gamma + \sin\theta\cos\gamma e^{i(\Delta\varphi+\Delta\phi+\phi_{dc}+\beta\sin\omega_m t)}\right) E_0 e^{-i\omega_c t} \\ &= \begin{bmatrix} \left(\cos\theta\sin\gamma + T_0 J_0(\beta)\sin\theta\cos\gamma e^{i\Delta\Phi}\right) \\ +\sin\theta\cos\gamma e^{i\Delta\Phi}\left(T_1 J_1(\beta) e^{-i\omega_m t} - T_{-1} J_1(\beta) e^{i\omega_m t}\right) \end{bmatrix} E_0 e^{-i\omega_c t} \end{aligned} \tag{5}$$

where $\Delta\Phi = \Delta\varphi + \Delta\phi + \phi_{dc}$. From Eq. (5), the upper part in the square bracket gives the carrier of modulated light and the lower part gives the two sidebands. The demodulated signal at frequency ω_m can be calculated as

$$\begin{aligned} I_{FM} &= e^{-2\delta_0} J_0(\beta) J_1(\beta) I_0 \sin^2\theta \sin^2\gamma \left[(\delta_{-1} - \delta_1)\sin\theta_{fm} - (\phi_1 + \phi_{-1} - 2\phi_0)\cos\theta_{fm}\right] \\ &+ \frac{1}{2} e^{-2\delta_0} J_1(\beta)\sin 2\theta \sin 2\gamma \left\{ \left[(\delta_{-1} - \delta_1)\cos\Delta\Phi + (\phi_{-1} - \phi_1)\sin\Delta\Phi\right]\sin\theta_{fm} \right. \\ &\left. - \left[(2 + 2\delta_0 - \delta_1 - \delta_{-1})\sin\Delta\Phi + (\phi_1 + \phi_{-1} - 2\phi_0)\cos\Delta\Phi\right]\cos\theta_{fm} \right\}. \end{aligned} \tag{6}$$

The expression of the first term (the first line) in Eq. (6) shows a pure FM signal. The other terms provide some distortion on the detected signal and a large offset overlaps in the signal according to the term $(2 + 2\delta_0 - \delta_1 - \delta_{-1})$. As can be seen, when $\Delta\Phi$ is zero, the expression of Eq. (6) can go to a pure FM spectroscopy with amplitude slightly larger than the first term. When there is no gas sample in the optical path, i.e., $\delta_{0,\pm1} = 0$ and $\phi_{0,\pm1} = 0$, the background signal caused by RAM can be deduced as

$$I_{RAM} = J_1(\beta) I_0 \sin 2\theta \cos 2\gamma \sin(\Delta\varphi + \Delta\phi + \phi_{dc})\cos\theta_{fm} \tag{7}$$

As can be seen, the amplitude of RAM shows a sine or cosine dependencies on the angle of the linear polarization direction of input laser and the *x*-axis θ, the angle of the *e*-axis of *f*-EOM and the output direction of the polarizer γ, the phase differences between the slow and fast axes of the PM fiber $\Delta\varphi$ and the EOM crystal $\Delta\phi$, the phase shift ϕ_{dc} induced by the external DC voltage, and the detection phase θ_{fm}. The amplitude of the RAM background signal could be zero and result in a pure FM signal by adjusting the value of the related parameters. In Section 3, a detailed examination of the dependences of RAM on the related parameters is given and also the results are compared with the theory.

Measurements of RAM

The experimental setup designed for measuring the dependences of RAM on the related parameters is shown in Fig. 2. The system was based on a distributed-feedback laser (DFB, NTT Electronics, NLK1S5GAAA) with a free-running line width of 2 MHz, working in the wavelength range from 1527 nm to 1529 nm. After the output of the laser source, a polarizer and a $\lambda/2$ wave plate were employed to control the state of polarization (SOP) and polarization orientation of the laser light. Then the laser light was coupled into a 2 m long PM fiber, the output of which was connected to an *f*-EOM (Photline, MPX-LN-05, bandwidth of DC-500 MHz) with titanium diffused waveguide and a DC response. Both temperatures of the PM fiber and the *f*-EOM were controlled by the temperature controller (Newport, Model 350B). The laser light output from the *f*-EOM impinged upon a fast response photodetector (*f*-PD, Newfocus, 1611-FS-AC-M) after passed through a second polarizer (the output polarizer). The detected signal was then amplified by a power amplifier (PA, Mini-Circuits, ZRL-700+). A 385 MHz RF driven source (New focus, 3363-A) was split into two parts, one of which was applied to the *f*-EOM via the RF input port of a Bias Tee (Mini-Circuits, ZFBT-4R2GW+, 0.1 Hz–4200 MHz) for providing the modulation signal, the other part of which was phase shifted by a phase shifter (Mini-Circuits, JSPHS 446+) and then went into a DBM (Mini-Circuits, ZLW-1) together with the detected signal. The demodulated signal was finally filtered by a low-pass filter (Mini-Circuits, cut frequency of 1.9 MHz) to yield the RAM signal.

Control variable method was adopted to measure the parameters dependences of RAM. The measurement of RAM as a function of the input linear polarization direction is shown in Fig. 3A with the angle of the output polarizer set to be 140°. From Eq. (7), the amplitude of RAM should dependent sinusoidally on the input linear polarization direction with a period of 180°; however the period becomes 90° in Fig. 3A since a half-wave plate was used to rotate the polarization direction of input laser light. The input polarization angles at which the amplitudes of RAM are zero represent that the linear polarization direction of the input laser is along the *x*- or *y*-axis, i.e., $\theta = n\pi/2$. Fig. 3B shows the measurement of RAM as a function of the angle of output polarizer when the angle of half-wave plate is fixed at 133°. As can be seen, the amplitude of RAM depends sinusoidally on the angle of output polarizer with a period of 180°, which is consistent with the theory shown in Eq. (7). The amplitude of RAM is almost zero when the angle of output polarizer is around 150°, corresponding to $\gamma = n\pi/2$ (n is an integer).

The temperature dependences of RAM were measured since the phase differences $\Delta\varphi$ and $\Delta\phi$ can be changed by temperature. In the experimental process, the angle of half-wave plate was fixed at 110° and the output polarizer was set around 60° corresponding to the maximum transmission. Fig. 4A shows the measured amplitude of RAM when the temperature of PM fiber was changed from 24 °C to 27.4 °C. The temperature of *f*-EOM was fixed at 25 °C. According to the temperature influence of PM fiber on the RAM, temperatures of 24 °C and 26.8 °C, at which RAM is close to zero, should be chosen. Fig. 4B shows the measurement of RAM as a function of the temperature of *f*-EOM with the PM fiber temperature stabilized at 24 °C. As can be seen, the temperature dependence of RAM shows a sinusoidal relationship and the period of *f*-EOM temperature dependence of RAM is much smaller than that of PM fiber.

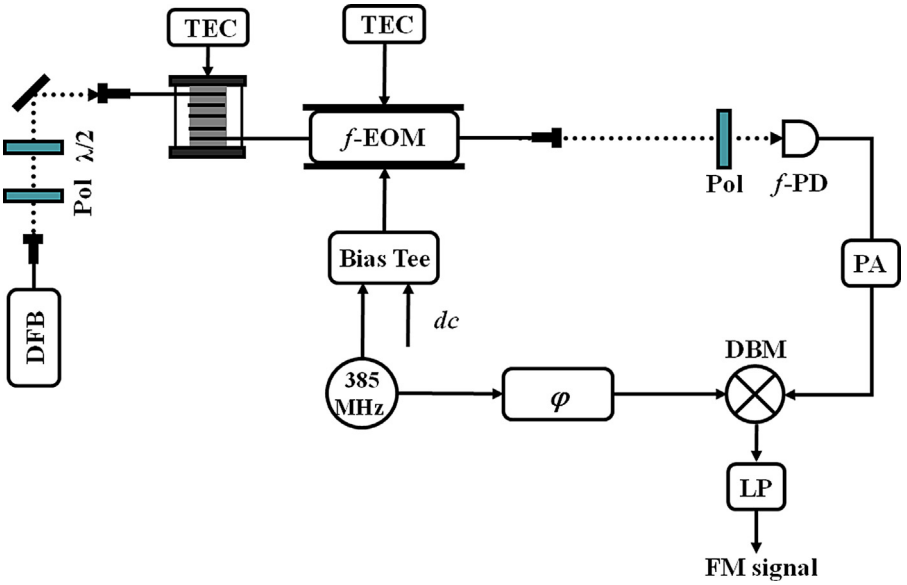

Fig. 2. Experimental setup for the measurements of RAM. DFB—distributed feedback laser; TEC—temperature controller; λ/2—half-wave plate; dc—DC voltage applied to *f*-EOM; PA—power amplifier.

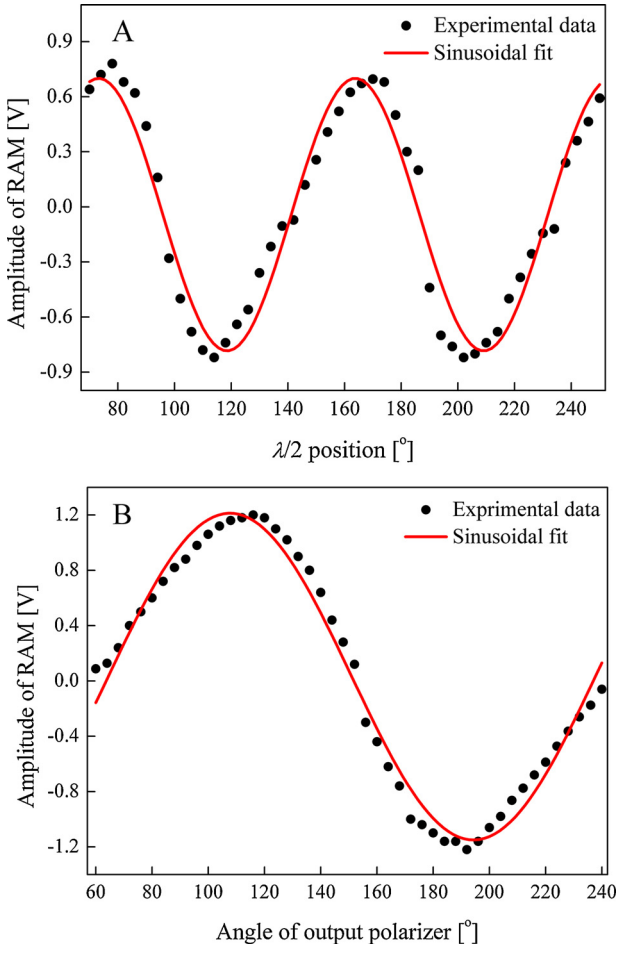

Fig. 3. Polarization dependence of RAM. (A) The amplitude of RAM as a function of the angle of half-wave plate. (B) The amplitude of RAM as a function of the angle of output polarizer.

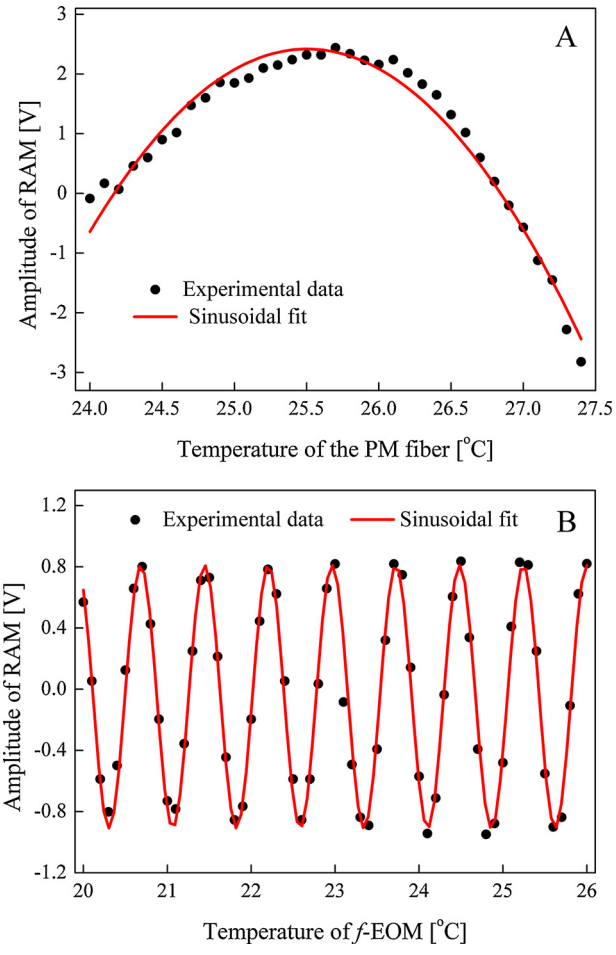

Fig. 4. Temperature dependences of RAM. Measurements of RAM (A) as a function of the temperature of PM fiber and (B) as a function of the temperature of *f*-EOM.

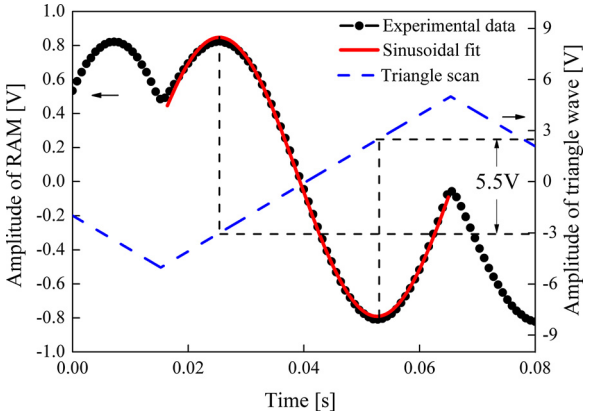

Fig. 5. Measurement of the dependence of RAM on the external DC voltage.

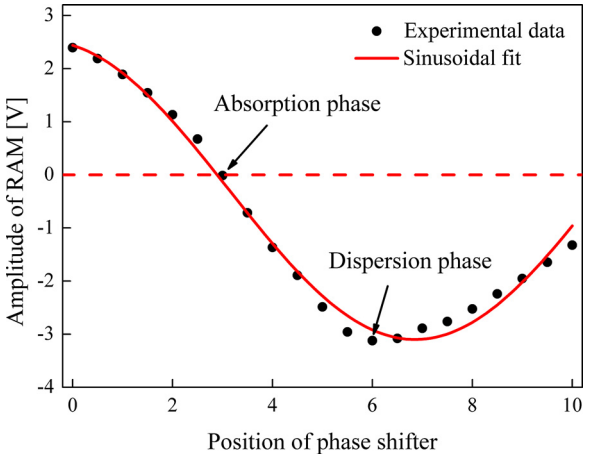

Fig. 6. The amplitude of RAM as a function of the knob position of phase shifter.

It means that a temperature variation of the *f*-EOM will affect the RAM more greatly than that of PM fiber.

In order to investigate the influence of the phase shift ϕ_{dc} on RAM, a triangle wave voltage signal at 10 Hz with amplitude of 10 V was applied the *f*-EOM via the DC input port of the Bias Tee together with the RF power. As shown in Fig. 5, the amplitude of RAM shows a sinusoidal dependence on the triangle wave voltage and the theoretical fit is in excellent agreement with the measured data, which indicate that the amplitude of RAM shows a fast linear response on the low frequency voltage signal applied to *f*-EOM. From the voltage response, we find that the half-wave voltage of the employed *f*-EOM is only 5.5 V.

The detection phase θ_{fm} is an important parameter to determine the gas information from FMS, and in general it is obtained by fitting the lineshape of FM signal [23]. In this paper, we find that the absorption or dispersion phase could be determined accurately when the RAM exists in FMS. According to Eq. (7), if a sine signal is added to the *f*-EOM, i.e., $\phi_{dc} = A\sin(\omega t)$ and A is the conversion factor between voltage and phase, the FM background signal only shows a cosine dependence on detection phase. Therefore, the phase with largest or zero magnitude corresponds to the dispersion phase or absorption phase. In Fig. 6, the dots represent the measurements of the amplitude of RAM as a function of the knob of phase shifter, which shows a sine or cosine function relationship corresponding to the expression in Eq. (7). As can be seen, positions 3 and 6 correspond to the absorption phase and dispersion phase, respectively. The error between experimental and theoretical fit is mainly because of the nonlinear variation of the phase shifter. When the phases were determined, the sine signal applied to *f*-EOM was removed.

Active servo control of RAM

Principle of our scheme

According to Eq. (7), the amplitude of RAM is related to the phase differences induced by the birefringence of the input PM fiber and EO crystal. Meanwhile, the phase differences can absolutely change the polarization state of the output light. So the RAM is certainly correlative to the polarization state variation of the modulated light caused by the birefringence effects. Fortunately, the phase difference ϕ_{dc} in the sin term could be controlled by an external DC voltage and used for compensating the natural birefringence effects, i.e., the magnitude of the RAM background signal could be zero by adjusting the applied external DC voltage. Consequently, the correction signal can be obtained through detecting the SOP of laser light before interaction with the gas sample by a polarization detection scheme, which was first invented and used for frequency stabilization by Hänsch and Couillaud [24].

The schematic description for reduction of RAM with active servo control is presented in Fig. 7. The DFB laser with single mode output was connected to the *f*-EOM with a flange. The output light from *f*-EOM was divided into two beams by a partially reflecting mirror. The transmitted part of light then entered into an absorption cell and interacted with the target gas sample. The reflected part of light was guided into the polarization detection scheme which is composed of a $\lambda/4$ wave plate (QWP), a polarization beam splitter (PBS), two DC detectors and a subtractor. The slow axis of QWP has an angle of 45° with respect to *y*-axis and the two output polarization directions of PBS are parallel to *x*- and *y*-axis, respectively. During this procedure, the accurate angle relationships are controlled by rotating the $\lambda/2$ wave plate and QWP to make the subtracted signal zero offset when a low frequency sinusoidal wave was applied to the *f*-EOM.

According to Eq. (4), the two electrical fields exiting the PBS can be written as

$$\begin{pmatrix} E_x \\ E_y \end{pmatrix} = J_{ROT}\left(\frac{\pi}{4}\right) J_{QWP} J_{EOM} \hat{E} = \frac{e^{-i\pi/4}}{2} \begin{pmatrix} \cos\theta(1+i) + \sin\theta e^{i(\Delta\varphi+\Delta\phi+\phi_{dc}+\beta\sin\omega_m t)}(1-i) \\ \cos\theta(1-i) + \sin\theta e^{i(\Delta\varphi+\Delta\phi+\phi_{dc}+\beta\sin\omega_m t)}(1+i) \end{pmatrix} E_0 e^{-i\omega t} \quad (8)$$

where $J_{ROT}(\alpha)$ is the rotation Jones Matrix with the rotation angle of α. The difference of the light intensities measured with the two DC detectors is derived as

$$I_x - I_y = 4I_0 \sin 2\theta \sin\left(\Delta\varphi + \Delta\phi + \phi_{dc} + \beta\sin\omega_m t\right). \quad (9)$$

Using Jacobi–Anger expansion, Eq. (9) can be represented as

$$I_x - I_y = 4I_0 \sin 2\theta \sin\left(\Delta\varphi + \Delta\phi + \phi_{dc} + \beta\sin\omega_m t\right) = 4I_0 \sin 2\theta \begin{bmatrix} J_0(\beta)\sin(\Delta\varphi + \Delta\phi + \phi_{dc}) \\ +2J_1\cos(\Delta\varphi + \Delta\phi + \phi_{dc})\sin\omega_m t \end{bmatrix}. \quad (10)$$

Since two slow response detectors are used, the intensity of the signal at modulation frequency cannot be detected. So Eq. (10) can be simplified as

$$I_x - I_y = 4J_0(\beta) I_0 \sin 2\theta \sin(\Delta\varphi + \Delta\phi + \phi_{dc}). \quad (11)$$

The expression of the error signal obtained from the polarization detection system is similar to Eq. (7), but with larger amplitude. After proposed by a PID (Stanford Research System, SR960), the

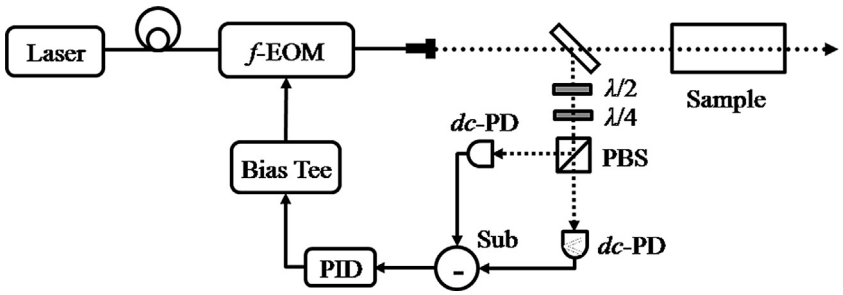

Fig. 7. Schematic description for the reduction of RAM with active servo control. PID—proportional–integral–derivative controller; Sub—subtractor; PBS—polarization beam splitter.

error signal with the bandwidth of 10 kHz, determined by the PID controller, will be applied to the *f*-EOM through the DC input port of the Bias Tee to control the phase difference of the birefringent material at low frequency.

Experimental results

In the theoretical analysis a new servo control method different from previous investigations is suggested to reduce RAM. The FM signals of C_2H_2 gas at the wavenumber of 6544.4419 cm^{-1}, with its line strength of 9.745×10^{-21} $cm^{-1}/(molecule\,cm^{-2})$ [25], were measured to examine the new strategy. The experimental setup was established based on the design shown in Fig. 2, in which the polarization detection system, the feedback loop, and the gas cell were added. The absorption cell was 5 cm long and the pressure of C_2H_2 gas was about 40 Torr which was obtained through the fitting results of direct absorption spectrum. During the experimental process, the temperature of PM fiber and *f*-EOM were fixed at 24 °C and 23.1 °C, respectively, to minimize the RAM. By adjusting the half-wave plate before *f*-EOM, the angle θ between the polarization direction of incident light and *x*-axis was set to be 10° to enhance the effect of non-perfect light entering. The angle γ was fixed at an angle of 20°.

The measurements of the FM signals are shown in Fig. 8, in which A and C display the absorption and dispersion signals without active servo control; B and D display the corresponding signals with active servo control. The frequency scale was calibrated using an optical cavity with the free spectral range of 381 MHz [26]. As can be seen, the lineshapes of signals are corrected and the offset in the dispersion signal is eliminated when the servo control loop is turned on.

In order to evaluate the stability of the feedback loop, the FM signals at the dispersion phase were measured with feedback loop off and on since the offset of dispersion signal is strictly related to the RAM. As shown in Fig. 9A, each measurement is implemented in a time period of 500 s. During the measurements, the fixed laser frequency was tuned far away from the transition line. When the feedback loop was off, the background signal shows a large offset and time-depending drift. When the feedback loop was turned on, the signal shows a constant value and zero offset. Fig. 9B shows the background stability described by Allan variance $\sigma(\tau)$. The dots and stars represent the $\sigma(\tau)$ with feedback loop on and off, respectively.

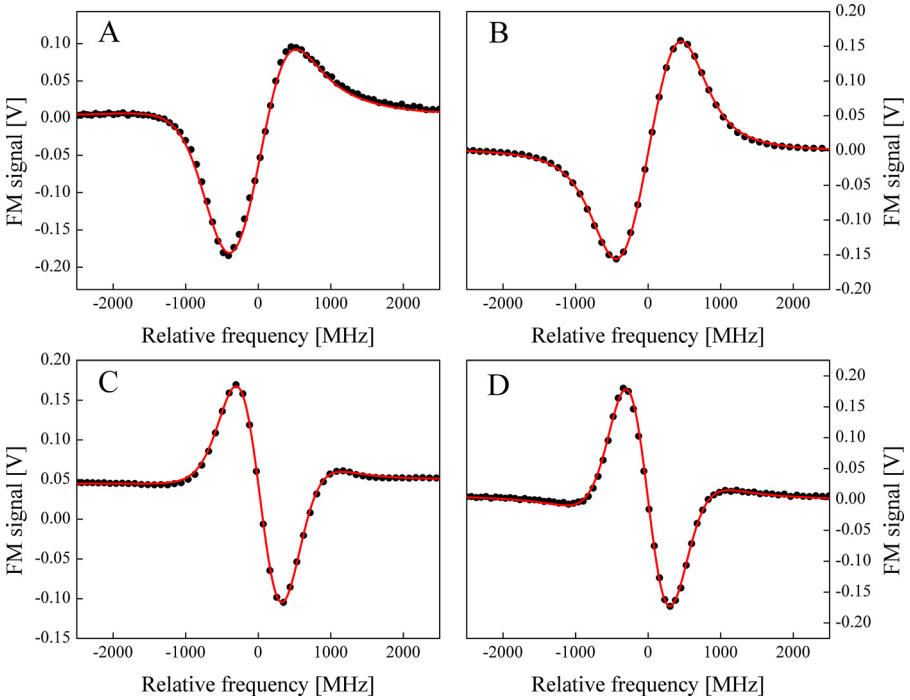

Fig. 8. Fitted results of FMS signal with absorption at knob 3 and dispersion at knob 6. (A) and (B) absorption signals; (C) and (D) dispersion signals. (A) and (C) with feedback loop off; (B) and (D) with feedback loop on.

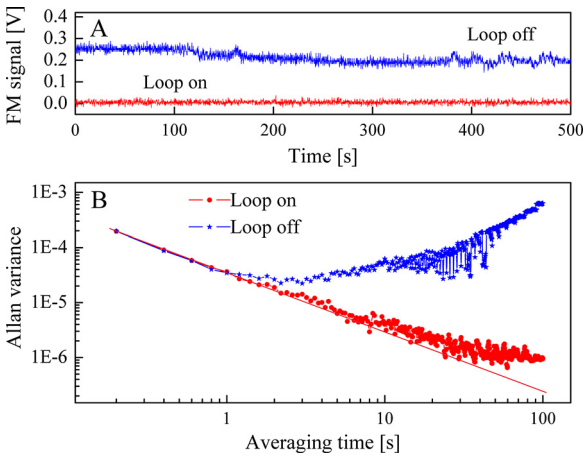

Fig. 9. Long term measurements of FM background signal with and without servo control and the stability analysis using Allan variance. (A) Typical background drift with feedback loop on and off. (B) The background stability described by the square root of Allan variance $\sigma(\tau)$.

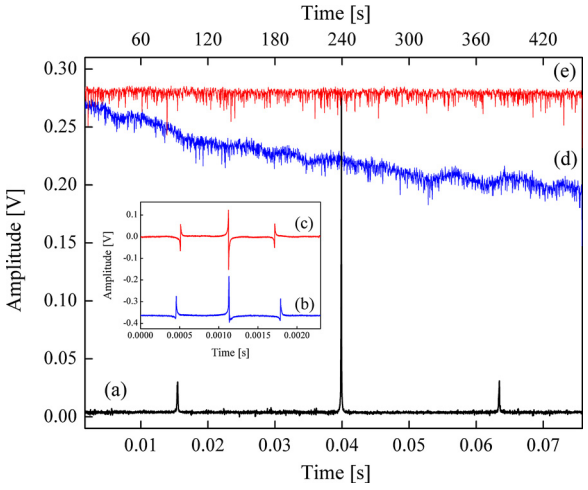

Fig. 10. Measurements of cavity transmission and error signal in PDH frequency stabilization.
(a) A group of typical cavity transmission of the modulated light composed of the carrier and two sidebands. (b) and (c) Error signals obtained with RAM control off and on. (d) and (e) Cavity transmission after laser frequency locked with RAM control off and on.

The solid line shows the $\tau^{-1/2}$ dependence for white noise. When the loop is off, the minimum $\sigma(\tau)$ is 2.232×10^{-5} at $\tau = 3$ s and shows a feature of random walk. When the loop is turned on, the minimum of $\sigma(\tau)$ is improved to 9×10^{-7} at $\tau = 100$ s and shows a nearly white noise dependence.

Application in Pound–Drever–Hall (PDH) technique

In PDH frequency stabilization technique, the error signal obtained from the optical heterodyne detection of cavity reflection could also be influenced by RAM generated in the FM process, which will result in a drift in frequency locking position and reduce the locking stability. Here the new proposed servo control method is adopted in the PDH technique to optimize the frequency stabilization. The experimental setup is similar to that employed in Ref. [2]. In our experimental setup, the *f*-EOM was used to modulate the laser frequency and the cavity used for previous frequency calibration in FMS with the mode width of about 100 kHz was employed [22]. Curve (a) in Fig. 10 shows a group of typical cavity transmission of the modulated light composed of the carrier and two sidebands. Curves (b) and (c) illustrated in Fig. 10 show the obtained error signals with RAM control off and on, respectively. As can be seen, the offset of the error signal is eliminated and the distortion is corrected when the RAM servo control is turned on. Curves (d) and (e) show the cavity transmission after the laser frequency is locked with RAM control off and on, respectively. The fluctuation of the light intensity of (d) is due to the drift of the frequency locking position caused by the temperature dependence of RAM on the error signal. With the RAM servo control on, the laser frequency was stabilized at the peak of the transmission mode and the transmitted light intensity shows a constant value, as shown in curve (e).

Conclusion

FMS is a highly sensitive technique for trace gas sensing, however its sensitivity is always limited by RAM induced in FM process. In this paper we focused on the RAM induced by nonlinear polarized light incident or imperfect alignment in the FM process. The theoretical expression for the detected signal in FMS with RAM contained was calculated by utilizing the Jones vectors. Then the dependent relationships between RAM and each parameter were experimentally measured and they were coincident with the theoretical results. In order to reduce the RAM, a novel servo control method was proposed to reduce the influence of RAM, in which the correction signal was obtained through detecting the light before interaction with gas sample using a polarization detection scheme. Under the new strategy, the FM signals of C_2H_2 at the wavenumber of 6544.4419 cm^{-1} was measured and pure FM lineshapes are obtained. Long-term measurements of the dispersion background signal with feedback loop on and off were performed and the square root of Allan variance $\sigma(\tau)$ is improved from 2.232×10^{-5} at $\tau = 3$ s to 9×10^{-7} at $\tau = 100$ s when the feedback loop is turned on. Finally, this servo control method is extended into the application of Pound–Drever–Hall frequency stabilization technique to improve the locking accuracy and stability. These investigations are useful for improving the detection sensitivity of FMS to trace gas detection.

Acknowledgments

This project was supported by the 973 program (Grant no. 2012CB921603), National Natural Science Foundation of China (Grant nos. 61127017, 61178009, 61108030, 61275213, 61378047, and 61205216), Shanxi Natural Science Foundation (Grant nos. 2012021022-1, and 2013021004-1), Shanxi Scholarship Council of China (2013-011 and 2013-01), and the National Fundamental Fund of Personnel Training (J1103210).

References

[1] G.C. Bjorklund, Frequency-modulation spectroscopy: a new method for measuring weak absorptions and dispersions, Optics Letters 5 (1) (1980) 15–17.
[2] R.W. Drever, J.L. Hall, V. Kowalski, J. Hough, G.M. Ford, A.J. Munley, H. Ward, Laser phase and frequency stabilization using an optical resonator, Applied Physics B: Lasers and optics 31 (1983) 97–105.
[3] C.B. Carlisle, D.E. Cooper, Tunable-diode-laser frequency-modulation spectroscopy using balanced homodyne detection, Optics Letters 14 (23) (1989) 1306–1308.
[4] C.M. Shum, E.A. Whittaker, Determination of radio-frequency phase in harmonic frequency modulation spectroscopy, Applied Optics 30 (27) (2001) 3799–3804.
[5] G.C. Bjorklund, M.D. Levenson, Sub-Doppler frequency-modulation spectroscopy of I_2, Physical Review A: Atomic, Molecular, and Optical Physics 24 (1) (1981) 166–169.
[6] J.A. Silver, Frequency-modulation spectroscopy for trace species detection: theory and comparison among experimental methods, Applied Optics 31 (6) (1992) 707–717.
[7] W.H. Oskay, S.A. Diddams, E.A. Donley, T.M. Fortier, T.P. Heavner, L. Hollberg, W.M. Itano, S.R. Jefferts, M.J. Delaney, K. Kim, F. Levi, T.E. Parker, J.C. Bergquist,

Single-atom optical clock with high accuracy, Physical Review Letters 97 (2) (2006) 020801.
[8] V. Negnevitsky, L.D. Turner, Wideband laser locking to an atomic reference with modulation transfer spectroscopy, Optics Express 21 (3) (2013) 3103–3113.
[9] T. Akutsu, S. Kawamura, A. Nishizawa, K. Arai, K. Yamamoto, D. Tatsumi, S. Nagano, E. Nishida, T. Chiba, R. Takahashi, N. Sugiyama, M. Fukushima, T. Yamazaki, M.K. Fujimoto, Search for a stochastic background of 100-MHz gravitational waves with laser interferometers, Physical Review Letters 101 (10) (2008), 101101.
[10] I. Ben-Aroya, M. Kahanov, G. Eisenstein, Multi-field frequency modulation spectroscopy, Optics Express 16 (9) (2008) 6081–6097.
[11] K. Ruxton, A.L. Chakraborty, W. Johnstone, M. Lengden, G. Stewart, K. Duffin, Tunable diode laser spectroscopy with wavelength modulation: elimination of residual amplitude modulation in a phasor decomposition approach, Sensors and Actuators B: Chemical 150 (2010) 367–375.
[12] M. Romagnoli, M.D. Levenson, G.C. Bjorklund, Frequency-modulation polarization spectroscopy, Optics Letters 8 (12) (1983) 635–637.
[13] F. du Burck, O. Lopez, Correction of the distortion in frequency modulation spectroscopy, Measurement Science and Technology 15 (2004) 1327–1336.
[14] M.D. Levenson, W.E. Moerner, D.E. Horne, FM spectroscopy detection of stimulated Raman gain, Optics Letters 8 (2) (1983) 108–110.
[15] N.C. Wong, J.L. Hall, Servo control of amplitude modulation in frequency-modulation spectroscopy: demonstration of shot-noise-limited detection, Journal of the Optical Society of America B: Optical Physics 2 (9) (1985) 1527–1533.
[16] D.E. Cooper, J.P. Watjen, Two-tone optical heterodyne spectroscopy with a tunable lead-salt diode laser, Optics Letters 11 (10) (1986) 606–608.
[17] S. Kasapi, S. Lathi, Y. Yamamoto, Amplitude-squeezed, frequency-modulated, tunable, diode-laser-based source for sub-shot-noise FM spectroscopy, Optics Letters 22 (7) (1997) 478–480.
[18] A. Foltynowicz, I. Silander, O. Axner, Reduction of background signals in fiber-based NICE-OHMS, Journal of the Optical Society of America B: Optical Physics 28 (11) (2011) 2797–2805.
[19] W. Ma, Z. Li, W. Tan, G. Zhao, X. Fu, L. Zhang, L. Dong, W. Yin, S. Jia, Servo control of highdegree of linear polarization output from polarization-maintaining fiber and its application in fiber-component based frequency modulation spectroscopy, Applied Physics Express 6 (2013) 112501.
[20] Z. Yin, Theoretical and experimental analysis of residual amplitude modulation in fiber-component-based frequency modulation spectrometry, in: Master Thesis, Umeå University, Umeå, Sweden, 2009.
[21] Private Communication with the Technical Engineer Herve Gouraud of Photline Corporation. herve.gouraud@photline.com
[22] I. Silander, P. Ehlers, J. Wang, O. Axner, Frequency modulation background signals from fiber-based electro optic modulators are caused by crosstalk, Journal of Optical Society of America B: Optical Physics 29 (5) (2012) 916–923.
[23] A. Foltynowicz, W.G. Ma, F.M. Schmidt, O. Axner, Doppler broadened noise-immune cavity-enhanced optical heterodyne molecular spectrometry signals from optically saturated transitions under low pressure conditions, Journal of the Optical Society of America B: Optical Physics 25 (7) (2008) 1156–1165.
[24] T.W. Hänsch, B. Couillaud, Laser frequency stabilization by polarization spectroscopy of a reflecting reference cavity, Optics Communications 35 (3) (1980) 441–444.
[25] HITRAN 2008 Database.(Version 12.0).
[26] Z. Li, W. Ma, X. Fu, W. Tan, G. Zhao, L. Dong, L. Zhang, W. Yin, S. Jia, Optics Express 21 (15) (2013) 17961–17971.

Biographies

Zhixin Li received his B.S. degree in physics from Shanxi University, China, in 2009. He is now pursuing the Ph.D. degree of atomic and molecular physics from the Institute of Laser Spectroscopy in Shanxi University. His research interests include gas sensors, precision spectroscopy, and laser spectroscopy technique.

Longhui Zhao is currently pursuing his B.S. degree in physics from Shanxi University, China.

Wei Tan received his B.S. degree in applied physics from Shanxi University, China, in 2010. He is now pursuing the Ph.D. degree of atomic and molecular physics from the Institute of Laser Spectroscopy in Shanxi University. His research interests include nonlinear frequency conversion and nonlinear optics.

Weiguang Ma received his Ph.D. degree in optics from Shanxi University, China, in 2005. 2006.4–2009.1, he worked as a post doctor in Department of Physics in Umeå University, Sweden. Now he is an associate professor of Shanxi University. His research interests include optical parameter oscillation, sum frequency generation, highly sensitive laser spectroscopy, and trace gas detection.

Gang Zhao received his B.S. degree in electronics from Shanxi University, China, in 2012. He is now pursuing the M.S. degree of atomic and molecular physics from the Institute of Laser Spectroscopy in Shanxi University. His research interest is optical sensing.

Xiaofang Fu received her B.S. degree in electronics from Taiyuan University of Technology, China, in 2011. She is now pursuing the M.S. degree of optical engineering from the Institute of Laser Spectroscopy in Shanxi University. Her research interest is optical sensing.

Lei Dong received his Ph.D. degree in optics from Shanxi University, China, in 2007. 2008.6–20011.12, he worked as a post doctor in Rice University, America. Now he is an associate professor of Shanxi University. His research interests include optical sensors, trace gas detection, and laser spectroscopy. He is a member of the Optical Society of America.

Lei Zhang received his Ph.D. degree in atomic and molecular physics from Shanxi University, China, in 2008. Now he is an associate professor of Shanxi University. His research interests include laser-induced breakdown spectroscopy and highly sensitive laser spectroscopy.

Wangbao Yin received his B.S. in physics from Shanxi University, China, in 1986, and the Ph.D. degree in laser spectrum laboratory from Shanxi University, China, in 2003. He is currently a professor in Institute of Laser Spectroscopy. His research interests are environmental sensors, flexible electronic packaging, and application of laser spectroscopy.

Suotang Jia received his B.S. degree in physics in 1986 and the M.S. degree in optics in 1989 from Shanxi University, China. He graduated with the Ph.D. degree for research on laser spectroscopy in 1994 from East China Normal University. Since 1996, he has worked as a visiting scholar in CNRS in France, University of Maryland, Yale University, University of Connecticut and so on. He now is a professor in Shanxi University and became the president of Shanxi University in 2012. His research interests include quantum optics, quantum information, ultracold atom and molecular, and application of laser spectroscopy.